

Contact and Momentum Distribution of the Unitary Fermi Gas

R. Rossi,^{1,*} T. Ohgoe,² E. Kozik,³ N. Prokof'ev,^{4,5} B. Svistunov,^{4,5,6} K. Van Houcke,¹ and F. Werner⁷

¹*Laboratoire de Physique Statistique, Ecole Normale Supérieure, Université PSL, Sorbonne Université, Université Paris Diderot, CNRS, Paris, France*

²*Department of Applied Physics, University of Tokyo, 7-3-1 Hongo, Bunkyo-ku, Tokyo 113-8656, Japan*

³*Physics Department, King's College, London WC2R 2LS, United Kingdom*

⁴*Department of Physics, University of Massachusetts, Amherst, MA 01003, USA*

⁵*National Research Center "Kurchatov Institute", 123182 Moscow, Russia*

⁶*Wilczek Quantum Center, School of Physics and Astronomy and T. D. Lee Institute, Shanghai Jiao Tong University, Shanghai 200240, China*

⁷*Laboratoire Kastler Brossel, Ecole Normale Supérieure, Université PSL, CNRS, Sorbonne Université, Collège de France, Paris, France*

(Dated: September 11, 2018)

A key quantity in strongly-interacting resonant Fermi gases is the contact \mathcal{C} , which characterizes numerous properties such as the momentum distribution at large momenta or the pair correlation function at short distances. The temperature dependence of \mathcal{C} was measured at unitarity, where existing theoretical predictions differ substantially even at the qualitative level. We report accurate data for the contact and the momentum distribution of the unitary gas in the normal phase, obtained by Bold Diagrammatic Monte Carlo and Borel resummation. Our results agree with experimental data within error bars and provide crucial benchmarks for the development of advanced theoretical treatments and precision measurements.

PACS numbers: 05.30.Fk, 67.85.Lm, 74.20.Fg

The resonant Fermi gas is a fundamental model of quantum many-body physics. It features a smooth crossover between fermionic and bosonic superfluidity, as predicted in the context of condensed matter physics [1–4] and confirmed by remarkable experiments on ultracold atomic Fermi gases near Feshbach resonances [5]. It is also relevant to neutron matter [6, 7] and high-energy physics [8], particularly in the central region of the crossover, around the unitary point where the scattering length diverges. As a result of the vanishing interaction range, resonant Fermi gases feature characteristic ultraviolet singularities governed by a single quantity called contact [4, 9–12]. In particular, for the homogeneous gas, the density-density correlation function at short distance diverges as

$$\langle \hat{n}_\uparrow(\mathbf{r}) \hat{n}_\downarrow(\mathbf{0}) \rangle \underset{r \rightarrow 0}{\sim} \frac{\mathcal{C}}{(4\pi r)^2} \quad (1)$$

and the momentum distribution has the tail

$$n_\sigma(\mathbf{k}) \underset{k \rightarrow \infty}{\sim} \frac{\mathcal{C}}{k^4}. \quad (2)$$

Here \mathcal{C} is the contact per unit volume, $\hat{n}_\sigma(\mathbf{r}) = \hat{\psi}_\sigma^\dagger(\mathbf{r})\hat{\psi}_\sigma(\mathbf{r})$ is the density operator, and the spin- σ momentum distribution $n_\sigma(\mathbf{k})$ is normalised to $\int n_\sigma(\mathbf{k})d^3k/(2\pi)^3 = n_\sigma = \langle \hat{n}_\sigma(\mathbf{r}) \rangle$. A direct manifestation of Eq. (1) is that in a unit volume, the number of pairs of fermions separated by a distance smaller than s is $\mathcal{C}s/(4\pi)$ in the $s \rightarrow 0$ limit. Hence \mathcal{C} controls the (anomalously high) density of pairs with vanishing interparticle distance [9, 11, 13].

A large variety of experimentally studied observables are directly expressible in terms of the contact: the population of the closed channel molecular state measured by laser molecular spectroscopy [14, 15], the large-momentum tail of the static structure factor measured by Bragg spectroscopy [16–18], the tail of the momentum distribution measured by non-interacting time-of-flight or by momentum-resolved radiofrequency spectroscopy [19], the derivative of the energy with respect to the inverse scattering length [10] extracted from the pressure equation of state measured by in-situ imaging [20], the large-frequency tail in radiofrequency spectroscopy [19, 21–23], and the short-distance density-density correlation function extracted from the three-body loss rate in presence of a bosonic cloud [24].

The experimental study [22] is particularly important because it is spatially resolved and for the first time yields the temperature dependence of the contact for a homogeneous system. Recently, two other experimental groups have presented preliminary data for the temperature-dependent homogeneous contact [25]. Understanding the experimental data remains a major challenge, because existing theoretical predictions, based on lowest order skeleton Feynman diagrams [26–28] or Monte Carlo simulations on a lattice [29, 30] contradict each other even at the qualitative level, especially on approach to the superfluid transition from the normal side.

In this Letter, we present high precision results for the contact of the unitary Fermi gas in the normal phase. We employ the Bold Diagrammatic Monte Carlo (BDMC) technique, in which all skeleton Feynman diagrams are

sampled stochastically up to a maximal order N_{\max} [31], and convergence towards the exact result in the limit $N_{\max} \rightarrow \infty$ is obtained by applying an appropriate conformal-Borel resummation to the divergent diagrammatic series [32]. Our results agree with experimental data within the uncertainty limits, and establish that the contact is a slowly decreasing function of temperature at fixed density in the normal phase. Furthermore we observe a non-Fermi liquid behavior in the momentum distribution.

We directly extract the contact from the pair propagator Γ thanks to the relation

$$\mathcal{C} = -\Gamma(\mathbf{r} = \mathbf{0}, \tau = 0^-) \quad (3)$$

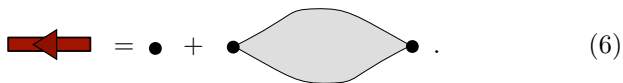
(we set \hbar and m to unity). While this relation was first obtained within T -matrix approximations [28, 33, 34], it actually becomes exact once Γ is fully dressed. Physically, this relation is consistent with the interpretation of \mathcal{C} in terms of a density of pairs, since it is formally analogous to the relation $n_\sigma = G_\sigma(\mathbf{r} = \mathbf{0}, \tau = 0^-)$ between the single-particle density and the single-particle propagator G . A simple way to derive Eq. (3) is to use the regularized version of Eq. (1) which holds in a lattice model [35],

$$\mathcal{C} = g_0^2 \langle \hat{n}_\uparrow(\mathbf{0}) \hat{n}_\downarrow(\mathbf{0}) \rangle \quad (4)$$

i.e. the contact is equal to the double occupancy, up to a renormalization factor set by the bare coupling constant g_0 (see also [13]). The result (3) then follows from the fact that

$$\Gamma(\mathbf{r}, \tau) = g_0 \delta(\tau) \frac{\delta_{\mathbf{r}, \mathbf{0}}}{b^3} - g_0^2 \langle T(\psi_\downarrow \psi_\uparrow)(\mathbf{r}, \tau) (\psi_\uparrow^\dagger \psi_\downarrow^\dagger)(\mathbf{0}, 0) \rangle \quad (5)$$

or, diagrammatically,



$$\text{thick red arrow} = \bullet + \bullet \text{---} \text{grey lens} \text{---} \bullet \quad (6)$$

Here $T[\dots]$ is the time-ordered product, and the first term does not contribute in the continuum limit where the lattice spacing b tends to zero.

Most results presented below were obtained using the bold scheme, where diagrams are built self-consistently from fully dressed propagators G and Γ ; when the temperature is not too low, we can alternatively use the non self-consistent ladder scheme, where diagrams are built from the non-interacting G_0 and ladder-sum Γ_0 [32, 36, 37]. By scale invariance, $\mathcal{C}\lambda^4$ is a universal function of $\beta\mu$, with μ the chemical potential, $\beta = (k_B T)^{-1}$ the inverse temperature, and $\lambda = \sqrt{2\pi\beta}$ the thermal wavelength. We have cross-checked the bold scheme against the ladder scheme at $\beta\mu = 0$, finding a relative difference for $\mathcal{C}\lambda^4$ smaller than 10^{-4} , well within the error bars. We typically went up to diagram order $N_{\max} = 9$ [60]. Without resummation, the bold

scheme with $N_{\max} = 1$ coincides with the self-consistent T -matrix approximation of Refs. [27, 38], and the ladder-scheme with $N_{\max} = 0$ coincides with the non-self-consistent T -matrix approximation of Ref. [26]. The non-resummed results oscillate wildly as a function of N_{\max} , which illustrates the absence of a small expansion parameter – *e. g.*, at $\beta\mu = 0$ for the ladder scheme, $\mathcal{C}\lambda^4$ changes by a factor ≈ 2 between $N_{\max} = 5$ and 6. We went down to $T/T_F \approx 0.19$, about 10% above the transition temperature to the superfluid phase $T_c/T_F \approx 0.17$ [39, 40]. Approaching closer to T_c requires tricks to stabilize the bold self-consistency loop, which we leave for future work.

Our results in the high-temperature region are shown in Fig. 1, together with the virial expansion

$$\mathcal{C}\lambda^4 = 16\pi^2 (c_2 e^{2\beta\mu} + c_3 e^{3\beta\mu} + \dots) \quad (7)$$

The coefficients $c_2 = 1/\pi$ [41] and $c_3 = -0.1399(1)$ [42, 43][61] come from the 2-body and 3-body problem respectively.

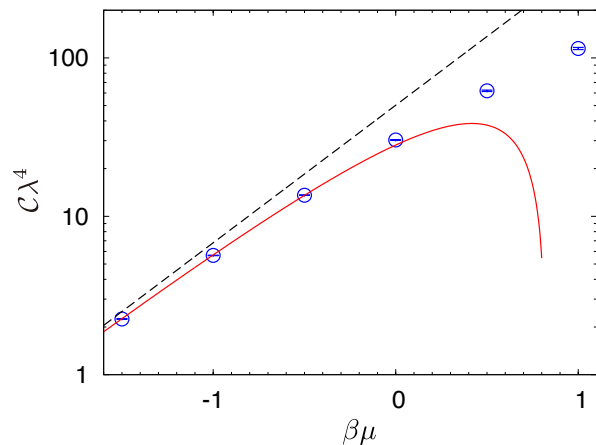


FIG. 1: The contact obtained by diagrammatic Monte Carlo (circles with error bars) agrees with the virial expansion [41, 42] at order two (dashed line) and three (solid line) in the high-temperature limit $\beta\mu \rightarrow -\infty$.

The behavior of the contact in the low-temperature region of the normal phase is displayed in Fig. 2. The contact in terms of canonical variables, $\mathcal{C}(n, T)$ or equivalently \mathcal{C}/k_F^4 versus T/T_F , is shown in Fig. 2a. We find a remarkably weak temperature dependence, which results from a compensation between two competing effects, as we will see from the momentum distribution below. The difference between the experimental results of Ref. [22] and our data is on the order of the experimental error bars, and the sign of this difference is essentially constant which indicates that the experimental error is mostly systematic rather than statistical. The lattice Auxiliary-Field Quantum Monte Carlo (AFQMC) data of Ref. [29] disagree with our results and predict an opposite temperature dependence; this may be due to a lack of control over systematic errors, whose main source is believed to

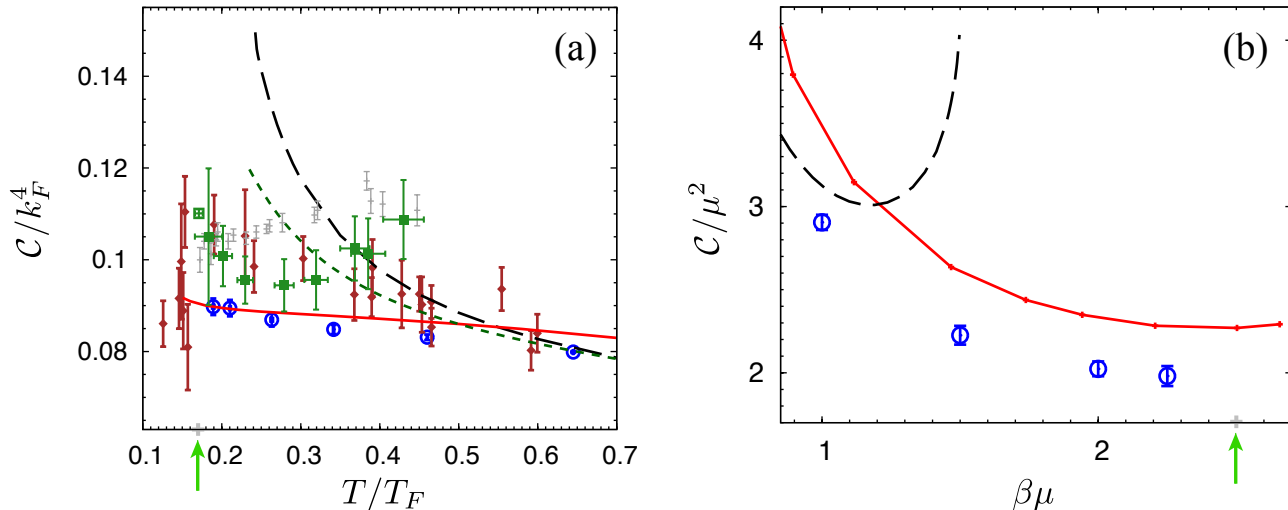


FIG. 2: Temperature dependence of the contact in the low-temperature region of the normal phase, in terms of (a) canonical and (b) grand canonical variables. BDMC (this work): blue solid circles, JILA experiment [22]: brown solid diamonds, lattice AFQMC simulations [29]: grey crosses, lattice DDMC with continuous-space and thermodynamic-limit extrapolations [30, 44]: green squares. The curves correspond to different diagrammatic approximations: non-self-consistent T -matrix [26]: dashed black line, self-consistent T -matrix [27]: solid red line, Nozières-Schmitt-Rink [28]: dotted green line in (a) and dashed black line in (b). The transition point to the superfluid phase [39, 40] is indicated by the green arrow.

be the discretization of space (i.e. the finite filling factor) [29]. The Determinantal Diagrammatic Monte Carlo (DDMC) data of Refs. [30, 44] have a non-monotonic temperature dependence which may also be an artifact of space-discretization errors, even though continuous-space extrapolation was performed. The data point at T_c from Ref. [44] (open square in Fig. 2) in combination with our data indicate that the slope $|d(C/k_F^4)/d(T/T_F)|$, which is much smaller than unity in the region $0.19 \lesssim T/T_F \lesssim 1$, quickly increases to values $\gtrsim 1$ on approach to the critical temperature [62]. This change of behavior may be related to the critical behavior [63]. The non-self-consistent T -matrix results of Ref. [26] and the Nozières-Schmitt-Rink results of Ref. [28] predict a more pronounced and gradual enhancement of the contact when decreasing temperature, which was interpreted in Ref. [26] as a manifestation of pseudogap physics. Our data demonstrate that this behavior is an artifact of the non-self-consistent T -matrix approach. The self-consistent T -matrix results of Ref. [27] are remarkably close to our data in Fig. 2a. In Fig. 2b we show the contact in terms of grand canonical variables, $\mathcal{C}(\mu, T)$ or equivalently C/μ^2 versus $\beta\mu$. It is natural to use these variables to discuss the different diagrammatic results since the diagrammatic technique is formulated in the grand-canonical ensemble. In this sense, the function $\mathcal{C}(n, T)$ is a combination of $\mathcal{C}(\mu, T)$ and of the equation of state $n(\mu, T)$, given for each of the considered approaches in Refs. [32, 45–47]. The non-self-consistent T -matrix and Nozières-Schmitt-Rink approaches yield the same result for $\mathcal{C}(\mu, T)$ (derivable from Eq. (3) by replacing the exact Γ with the sum of the ladder diagrams built on ideal-gas propagators), featuring again a strong enhancement at low temperature in dis-

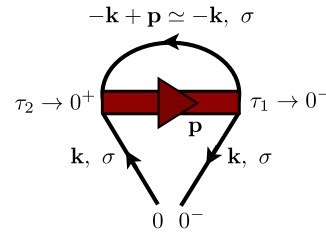


FIG. 3: Leading diagrammatic contribution to the momentum distribution $n_\sigma(\mathbf{k})$ at large k , which can be interpreted physically as the simultaneous propagation of two opposite-spin particles of large and nearly opposite momenta and of a missing pair of lower momentum $p \ll k$. Imaginary time runs from right to left. The single-particle lines propagate forward in time and can be replaced by vacuum propagators. The pair propagator runs backwards in time and is fully dressed.

agreement with our results. The self-consistent T -matrix data follows the same trend as ours up to a difference of about 20%. This difference largely cancels out with the difference in $n(\mu, T)$ when one considers $\mathcal{C}(n, T)$ as in Fig. 2a.

We turn to the momentum distribution, and begin with an analytic observation. The tail of the momentum distribution comes exclusively from the diagram of Fig. 3. Contributions from higher-order diagrams are suppressed, because integrations over internal times are restricted to narrow ranges, G and Γ being narrow functions of time at large momentum. The corresponding

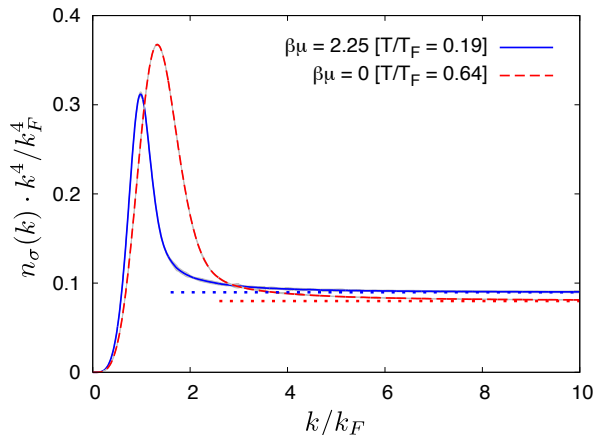


FIG. 4: BDMC data for the momentum distribution $n_\sigma(k)$, multiplied by k^4 in order to reveal the large-momentum tail $n_\sigma(k) \sim \mathcal{C}/k^4$. Dotted horizontal lines: values of the contact \mathcal{C} computed directly from the pair propagator. The uncertainties are represented by the grey error bands.

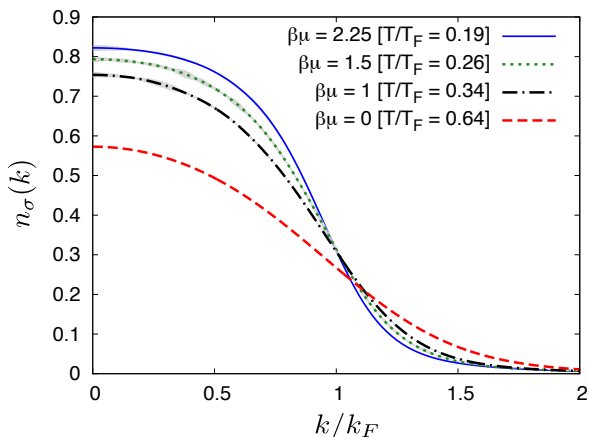


FIG. 5: BDMC data for the momentum distribution at various temperatures. Error bars are represented by the grey error bands.

asymptotic behavior of the self-energy is [64] [65]

$$\Sigma(\mathbf{k}, \tau) \simeq \mathcal{C} e^{\epsilon_{\mathbf{k}} \tau}, \quad k \rightarrow \infty, \tau \rightarrow 0^-. \quad (8)$$

This analytical understanding is readily incorporated into our BDMC scheme. The \mathcal{C}/k^4 tail of the momentum distribution is automatically built in provided we evaluate the lowest order self-energy diagram with high precision. To do so, we do not use Monte Carlo sampling, but rather the numerical procedure of Ref. [38], the only essential difference being that in our case, the pair propagator Γ which enters the numerical procedure is the fully dressed one.

The momentum distribution times k^4 is shown in Fig. 4 for two different temperatures. The large-momentum tail is reproduced without k -dependent statistical noise—in sharp contrast to other Monte Carlo methods [29, 48]—and perfectly agrees with our value of the contact deter-

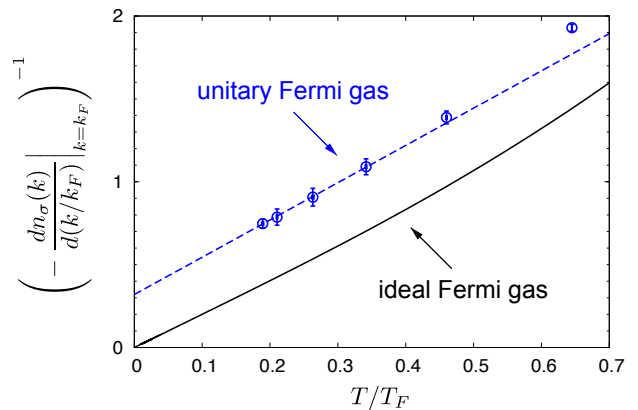


FIG. 6: Inverse slope of the momentum distribution at the Fermi momentum *vs.* temperature. For a Fermi liquid this quantity linearly tends to zero for $T/T_F \rightarrow 0$ (see solid line). In contrast, a linear extrapolation of our data for the unitary Fermi gas (dashed line) does not go through the origin.

mined from Eq. (3). One can note that the \mathcal{C}/k^4 tail contains as much as 10 to 15 percent of the particles. Finally, the momentum distribution at four different temperatures is shown in Fig. 5. The temperature dependence of $n_\sigma(k)$ is rather weak for the lowest three temperatures, but there is no sharp feature around k_F as would be the case for a pronounced degenerate Fermi liquid behavior. The smoothness of $n_\sigma(k)$ cannot be explained by finite-temperature Fermi-liquid theory: In a Fermi liquid the slope $dn_\sigma(k)/d(k/k_F)|_{k=k_F}$ would extrapolate to $-\infty$ in the limit $T/T_F \rightarrow 0$, and this does not occur for the unitary Fermi gas as shown by our data in Fig. 6. Deviations from Fermi liquid theory are also present in the equation of state, *e.g.* the specific heat is not linear in temperature [39]. Going to the largest temperature of Fig. 5, the low-momentum occupation numbers become much more depleted and the distribution broadens. However, the contact \mathcal{C}/k_F^4 is roughly unchanged (cf. Fig. 2a), which can be viewed as a delicate compensation between two trends: The occupation numbers increase for k moderately larger than k_F , which tends to increase the contact, but the onset of the \mathcal{C}/k^4 regime is pushed to higher momenta (see Fig. 4), which tends to decrease the contact.

In conclusion, we obtained accurate results for the temperature dependence of the contact and the momentum distribution of the normal unitary Fermi gas. This allows to discriminate between the contradicting earlier predictions. In the canonical ensemble, the contact is found to depend only weakly on temperature in a broad temperature range $T \lesssim T_F$, in remarkable agreement with the self-consistent T -matrix approximation [27]. The experimental data [22] are also consistent with our results given the experimental error bars [66]. More accurate experimental data are highly desirable to provide a more stringent test of our theoretical approach, and to understand the behavior of the contact when crossing the su-

perfluid phase transition [22]. Our results can also serve as benchmarks in numerous contexts where the contact appears in sum rules [9, 49–51] or in ultraviolet asymptotics [27, 51–56].

Acknowledgements. We thank F. Chevy for fruitful discussions. The data of Refs. [22, 26–30, 42, 44–47] were kindly provided by their authors. This work was supported by ERC grants Thermodynamix and Critisup2 (FW), a PICS from CNRS (FW, NP and BS), National Science Foundation under grant DMR-1720465 and MURI Program “Advanced quantum materials – a new frontier for ultracold atoms” from AFOSR (NP and BS), and the Simons Collaboration on the Many Electron Problem (EK, NP and BS). TO was supported by the MEXT HPCI Strategic Programs for Innovative Research (SPIRE), the Computational Materials Science Initiative (CMSI) and Creation of New Functional Devices and High-Performance Materials to Support Next Generation Industries (CDMSI), and by a Grant-in-Aid for Scientific Research (No. 22104010, 22340090, 16H06345 and 18K13477) from MEXT, Japan. Simulations ran on clusters at LKB-LPTMC/UPMC, UMass, the Supercomputer Center of the Institute for Solid State Physics at the University of Tokyo, and on the K computer provided by the RIKEN Advanced Institute for Computational Science under the HPCI System Research project (project number hp130007, hp140215, hp150211, hp160201, and hp170263). We acknowledge the hospitality of the Institute for Nuclear Theory, Seattle, the Aspen Center for Physics, and Mainz Institute for Theoretical Physics.

* Present address: Center for Computational Quantum Physics, The Flatiron Institute, New York, USA.

- [1] A. J. Leggett, in: A. Pekalski, J. Przystawa (eds.), *Modern Trends in the Theory of Condensed Matter*, p. 13. Springer, New York (1980).
- [2] A. J. Leggett, *J. Phys. (Paris)* **42**, C7 (1980).
- [3] P. Nozières and S. Schmitt-Rink, *J. Low Temp. Phys.* **59**, 195 (1985).
- [4] A. J. Leggett and S. Zhang, *Lecture Notes in Physics* **836**, 33 (2012), in [5].
- [5] *The BCS-BEC Crossover and the Unitary Fermi Gas*, *Lecture Notes in Physics* **836**, W. Zwerger ed. (Springer, Heidelberg, 2012).
- [6] J. Carlson, S. Gandolfi, and A. Gezerlis, *Prog. Theor. Exp. Phys.* **2012**, 01A209 (2012).
- [7] G. C. Strinati, P. Pieri, G. Roepke, P. Schuck, and M. Urban, *Phys. Rep.* **738**, 1 (2018).
- [8] *New J. Phys* **14** (2011), *Focus on Strongly Correlated Quantum Fluids: from Ultracold Quantum Gases to QCD Plasmas*, A. Adams, L. D. Carr, T. Schaefer, P. Steinberg, J. E. Thomas (eds.).
- [9] S. Tan, *Ann. Phys.* **323**, 2952 (2008).
- [10] S. Tan, *Ann. Phys.* **323**, 2971 (2008).
- [11] E. Braaten, *Lecture Notes in Physics* **836**, 193 (2012), in [5].
- [12] Y. Castin and F. Werner, *Lecture Notes in Physics* **836**, 127 (2012), in [5].
- [13] E. Braaten and L. Platter, *Phys. Rev. Lett.* **100**, 205301 (2008).
- [14] G. B. Partridge, K. E. Strecker, R. I. Kamar, M. W. Jack, and R. G. Hulet, *Phys. Rev. Lett.* **95**, 020404 (2005).
- [15] F. Werner, L. Tarruell, and Y. Castin, *Eur. Phys. J. B* **68**, 401 (2009).
- [16] E. D. Kuhnle, H. Hu, X.-J. Liu, P. Dyke, M. Mark, P. D. Drummond, P. Hannaford, and C. J. Vale, *Phys. Rev. Lett.* **105**, 070402 (2010).
- [17] E. D. Kuhnle, S. Hoinka, P. Dyke, H. Hu, P. Hannaford, and C. J. Vale, *Phys. Rev. Lett.* **106**, 170402 (2011).
- [18] S. Hoinka, M. Lingham, K. Fenech, H. Hu, C. J. Vale, J. E. Drut, and S. Gandolfi, *Phys. Rev. Lett.* **110**, 055305 (2013).
- [19] J. T. Stewart, J. P. Gaebler, T. E. Drake, and D. S. Jin, *Phys. Rev. Lett.* **104**, 235301 (2010).
- [20] N. Navon, S. Nascimbène, F. Chevy, and C. Salomon, *Science* **328**, 729 (2010).
- [21] W. Schneider and M. Randeria, *Phys. Rev. A* **81**, 021601(R) (2010).
- [22] Y. Sagi, T. E. Drake, R. Paudel, and D. S. Jin, *Phys. Rev. Lett.* **109**, 220402 (2012).
- [23] C. Shkedrov, Y. Florshaim, G. Ness, A. Gandman, and Y. Sagi, *High Sensitivity RF Spectroscopy of a Strongly-Interacting Fermi Gas*, arXiv:1803.01770.
- [24] S. Laurent, M. Pierce, M. Delehaye, T. Yefsah, F. Chevy, and C. Salomon, *Phys. Rev. Lett.* **118**, 103403 (2017).
- [25] Talk by C. Vale (Swinburne University) and poster by J. Struck (MIT) at the conference *BEC 2017 - Frontiers in Quantum Gases*, Sant Feliu de Guixols, Spain.
- [26] F. Palestini, A. Perali, P. Pieri, and G. C. Strinati, *Phys. Rev. A* **82**, 021605(R) (2010).
- [27] T. Enss, R. Haussmann, and W. Zwerger, *Ann. Phys.* **326**, 770 (2011).
- [28] H. Hu, X.-J. Liu, and P. D. Drummond, *New J. Phys.* **13**, 035007 (2011).
- [29] J. E. Drut, T. A. Lähde, and T. Ten, *Phys. Rev. Lett.* **106**, 205302 (2011).
- [30] O. Goulko and M. Wingate, *Phys. Rev. A* **93**, 053604 (2016).
- [31] K. Van Houcke, F. Werner, E. Kozik, N. Prokof'ev, B. Svistunov, M. J. H. Ku, A. T. Sommer, L. W. Cheuk, A. Schirotzek, and M. W. Zwierlein, *Nature Phys.* **8**, 366 (2012).
- [32] R. Rossi, T. Ohgoe, K. Van Houcke, and F. Werner, *Resummation of diagrammatic series with zero convergence radius for strongly correlated fermions*, arXiv:1802.07717.
- [33] P. Pieri, A. Perali, and G. C. Strinati, *Nature Physics* **5**, 736 (2009).
- [34] R. Haussmann, M. Punk, and W. Zwerger, *Phys. Rev. A* **80**, 063612 (2009).
- [35] F. Werner and Y. Castin, *Phys. Rev. A* **86**, 013626 (2012).
- [36] K. Van Houcke, F. Werner, N. Prokof'ev, and B. Svistunov, *Bold diagrammatic Monte Carlo for the resonant Fermi gas*, arXiv:1305.3901.
- [37] R. Rossi, T. Ohgoe, K. Van Houcke, and F. Werner, in preparation.
- [38] R. Haussmann, *Phys. Rev. B* **49**, 12975 (1994).
- [39] M. J. H. Ku, A. Sommer, L. W. Cheuk, and M. W. Zwierlein, *Science* **335**, 563 (2012).

- [40] O. Goulko and M. Wingate, Phys. Rev. A **82**, 053621 (2010); E. Burovski, N. Prokofev, B. Svistunov, M. Troyer, Phys. Rev. Lett. **96**, 160402 (2006).
- [41] Z. Yu, G. M. Bruun, and G. Baym, Phys. Rev. A **80**, 023615 (2009).
- [42] M. Sun and X. Leyronas, Phys. Rev. A **92**, 053611 (2015).
- [43] X. Leyronas, *private communication*.
- [44] O. Goulko and M. Wingate, PoS Lattice2010 **187** (2010).
- [45] G. C. Strinati, Lecture Notes in Physics **836**, 99 (2012).
- [46] R. Haussmann, W. Rantner, S. Cerrito, and W. Zwerger, Phys. Rev. A **75**, 023610 (2007).
- [47] H. Hu, X.-J. Liu, and P. D. Drummond, Phys. Rev. A **77**, 061605(R) (2008).
- [48] S. Gandolfi, K. E. Schmidt, and J. Carlson, Phys. Rev. A **83**, 041601(R) (2011).
- [49] M. Punk and W. Zwerger, Phys. Rev. Lett. **99**, 170404 (2007).
- [50] G. Baym, C. J. Pethick, Z. Yu, and M. W. Zwiernik, Phys. Rev. Lett. **99**, 190407 (2007).
- [51] E. Taylor and M. Randeria, Phys. Rev. A **81**, 053610 (2010).
- [52] D. T. Son and E. G. Thompson, Phys. Rev. A **81**, 063634 (2010).
- [53] W. D. Goldberger and I. Z. Rothstein, Phys. Rev. A **85**, 013613 (2012).
- [54] Y. Nishida, Phys. Rev. A **85**, 053643 (2012).
- [55] T. Enss and R. Haussmann, Phys. Rev. Lett. **109**, 195303 (2012).
- [56] J. Hofmann, Phys. Rev. A **84**, 043603 (2011).
- [57] M. Campostrini, M. Hasenbusch, A. Pelissetto, and E. Vicari, Phys. Rev. B **74**, 144506 (2006).
- [58] M. Hasenbusch, J. Stat. Mech. **2006**, P08019 (2006).
- [59] R. Combescot, F. Alzetto, and X. Leyronas, Phys. Rev. A **79**, 053640 (2009).
- [60] See Supplemental Material for our data in numerical form, as well as plots showing the dependence on N_{\max} and a more detailed comparison with the virial expansion.
- [61] See also Ref. [28] which finds $c_3 \simeq -0.141$.
- [62] In Ref. [44], the result $\mathcal{C}/k_F^4 = 0.110(1)$ at T_c was obtained by a linear extrapolation of \mathcal{C}/k_F^4 vs. $\nu^{1/3}$ where ν is the filling factor. Using a quadratic extrapolation gives 0.105(5) which leads to the same qualitative conclusion.
- [63] The leading singular part is $\mathcal{C}_{\text{sing}}(T) \sim \pm A_{\pm} |T - T_c|^{1-\alpha}$ for $T \rightarrow T_c^{\pm}$ with $\alpha = -0.0151(3)$ and $A_+/A_- = 1.061(2)$ for the $U(1)$ universality class [57, 58].
- [64] See Ref. [36] for detailed derivations, and Refs. [28, 59] for related discussions restricted to the framework of T -matrix approximations.
- [65] Equation (8) can be rederived starting from Eq. (3.36) of [54] (Y. Nishida, *private communication*).
- [66] New preliminary experimental data from MIT are also in agreement with our results (J. Struck, *private communication*).